In Situ Transmission Electron Microscopy Investigation of the Electrochemical Lithiation–Delithiation of Individual Co_9S_8/Co-Filled Carbon Nanotubes

Qingmei Su,[†,‡] Gaohui Du,[*,†] Jun Zhang,[†] Yijun Zhong,[†] Bingshe Xu,[‡] Yuehai Yang,[§] Suman Neupane,[§] Kamal Kadel,[§] and Wenzhi Li[*,§]

[†]Institute of Physical Chemistry, Zhejiang Normal University, Jinhua 321004, China, [‡]College of Materials Science and Engineering, Taiyuan University of Technology, Taiyuan 030024, Shanxi, China, and [§]Department of Physics, Florida International University, Miami, Florida 33199, United States

ABSTRACT Carbon nanotube (CNT)-encapsulated metal sulfides/oxides are promising candidates for application as anode materials in lithium ion battery (LIB), while their electrochemical behavior and mechanism still remain unclear. A comprehensive understanding of the lithiation mechanism at nanoscale of this type of composites will benefit the design and development of high-performance LIB materials. Here, we use Co_9S_8/Co nanowire-filled CNTs as a model material to investigate the lithium storage mechanism by in situ transmission electron microscopy. For a Co_9S_8/Co nanowire-filled closed CNT, the reaction front propagates progressively during lithiation, causing an axial elongation of 4.5% and a radial expansion of 32.4%, while the lithiated nanowire core is still confined inside the CNT. Contrastingly, for an open CNT, the lithiated Co_9S_8 nanowire shows an axial elongation of 94.2% and is extruded out from the open CNT. In particular, a thin graphite shell is drawn out from the CNT wall by the extruded lithiated Co_9S_8. The thin graphite shell confines the extruded filler and protects the filler from pulverization in the following lithiation–delithiation cycles. During multiple cycles, the Co segment remains intact while the Co_9S_8 exhibits a reversible transformation between Co_9S_8 and Co nanograins. Our observations provide direct electrochemical behavior and mechanism that govern the CNT-based anode performance in LIBs.

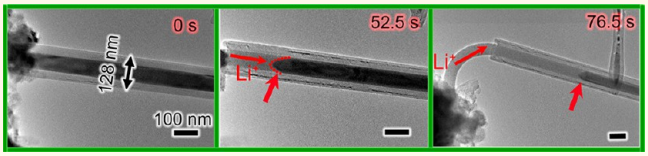

KEYWORDS: carbon nanotube · cobalt sulfide · lithiation · lithium ion battery · in situ TEM

Lithium ion batteries (LIBs) have an increasingly diverse range of applications from cars to microchips[1,2] and are currently the dominant power sources for portable electronic devices.[3,4] To meet the various applications, LIBs are required to have superior energy density, power density, and good cyclability.[5,6] LIBs deliver and store energy through reversible movement of Li^+ ions between the cathode and anode across an electrolyte-filled separator. Ultimately, the performance of LIBs depends on electrochemical behavior of the electrode materials. After the report of reversible Li^+ insertion into TiS_2 for LIBs by Whittingham in 1976,[7] many other transition metal dichalcogenides (or nitrides, phosphides, and fluorides), similar to metal oxides, were extensively investigated as anode materials for LIBs.[8−10]

Cobalt sulfide presents one of the promising anode materials to replace the carbonous anodes for the next-generation LIBs as it has a high theoretical lithium storage capacity (539 mAh/g for Co_9S_8),[11] which is larger than that of the carbonaceous anodes (372 mAh/g for graphite) currently used in commercial LIBs. However, unlike the small volume change (usually less than 10%) in an intercalation anode such as graphite, huge volume change inevitably occurs in metal sulfides or oxides anodes.[12,13] Such volume change generates large lithiation-induced strain and causes fracture and pulverization of the electrodes.[14] Metal sulfide or oxide anodes exhibit rapid capacity fading, even at low current densities, because of the large volume changes and the low conductivity during the discharging and charging processes. To mitigate these adverse effects for better capacity retention, several measures could be applied, for instance, by making hollow or porous nanostructures to adapt the volume change,[4,6,15]

* Address correspondence to gaohuidu@zjnu.edu.cn, wenzhi.li@fiu.edu.

Received for review October 9, 2013 and accepted November 19, 2013.

Published online November 19, 2013
10.1021/nn405254n

adding an elastomeric binder as a buffer,[16,17] or encapsulating the material in a conductive sheath such as carbon nanotubes (CNTs).[18,19] It was reported that carbon-coated cobalt sulfides show much higher specific capacity and good reversibility as compared to the noncoated ones.[20] CNT-based composites have attracted great attention as anode materials for LIBs due to the increased electrical conductivity and the enhanced mechanical strength offered by the carbon layers. In spite of the many efforts to improve the electrochemical performance, the knowledge about the microscopic electrochemical process of the electrode in LIBs is still very meager since the conventional techniques to analyze electrode materials, such as coin cell assembly, cyclic voltammetry, and galvanostatic charge/discharge, cannot provide direct evidence for the dynamic electrochemical behaviors in the charge–discharge cycles. Recently, in situ characterization methods have been developed to provide useful information on the reaction process in LIBs.[21−23] In particular, in situ transmission electron microscopy (TEM) study has the advantage of providing direct insights into the dynamic conversion of the lithiation and delithiation processes, and has the ability to realize the real-time observation of the microstructure evolution during electrochemical reaction.[12,24−28] Direct visualization of the lithiation process can unfold the operation mechanism of LIBs, provide important insight into how LIBs work, and guide the design and development of advanced LIBs for future applications.

In this work, we created an all-solid nano-LIB inside a TEM using an individual Co_9S_8/Co-filled CNT as the working electrode, and directly observed its lithiation and delithiation process for the first time. The microstructure evolution of the Co_9S_8/Co-filled CNT electrode was monitored by simultaneous determination with TEM and electron diffraction (ED). An in-depth understanding of the electrochemical process of CNT–base composite in LIB has been achieved.

RESULTS AND DISCUSSION

The in situ nanoscale electrochemical setup was schematically illustrated in Figure 1a and described in the Experimental Section. Briefly, the electrochemical nano-LIB constructed in the TEM consists of three parts: Co_9S_8/Co-filled CNT electrode, Li counter electrode, and Li_2O solid electrolyte. The Co_9S_8/Co-filled CNT samples were synthesized using Co/MgO as catalyst by a thermal chemical vapor deposition method as reported elsewhere.[29] The filling of the Co_9S_8 nanowires was resulted from the volume expansion when cobalt inside the CNT was transformed to cobalt sulfide and the extrusion action of CNTs as nanomolds. Due to the incomplete transition, sometimes Co nanoparticles could remain and be encapsulated together with Co_9S_8 by carbon shells. The majority of the Co_9S_8 nanowires encapsulated in the CNTs are 1–6 μm in length and

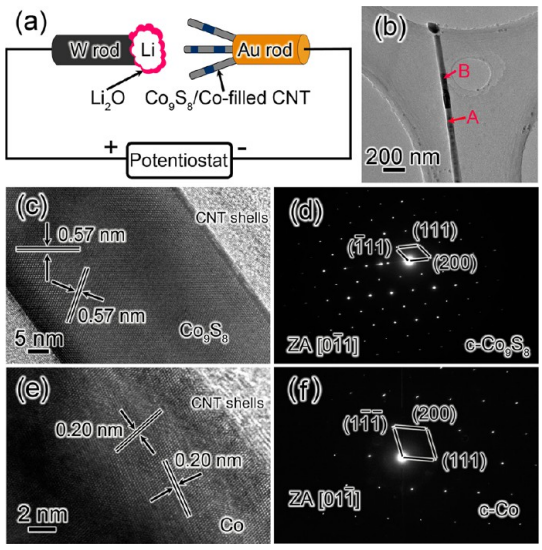

Figure 1. (a) Schematic illustration of the experimental setup for *in situ* TEM analysis of nano-LIB. (b) TEM image of a pristine Co_9S_8/Co-filled CNT consisting of two different regions, Co_9S_8 and Co, which are marked with letters A and B, respectively. (c) HRTEM image and (d) EDP of region A, confirming the Co_9S_8 phase. (e) HRTEM image and (f) EDP of region B, confirming the Co phase.

about 30–45 nm in diameter. Figure 1b shows a TEM image of a typical Co_9S_8/Co-filled CNT used in this study. The CNT shows different contrast in regions A and B, suggesting a heterogeneous filling within the CNT. The HRTEM image of region A is shown in Figure 1c. The boundary between the filling material and CNT is clear, and the core is a single-crystalline phase with fringe spacing of 0.57 nm, corresponding to the (111) planes of Co_9S_8. Figure 1d displays the electron diffraction pattern (EDP) of region A; the sharp spots could be well indexed as (200), (111), and (−111) planes of cubic Co_9S_8 (a = 9.923 Å, JCPDF card No. 86–2273) along the [0 −1 1] zone axis. The HRTEM image of region B is given in Figure 1e; the fringe spacing of 0.20 nm is agreed with the (111) plane of cubic Co. The structure is further confirmed by EDP (Figure 1f), which can be well indexed to the (111), (200) and (1 −1 −1) planes of cubic Co along the [0 1 −1] zone axis (a = 3.545, JCPDF card No. 15–0806). The thorough analysis of the sample reveals that the Co_9S_8 nanowires are largely encapsulated within the CNTs with the presence of a small amount of short Co segments. For the design of advanced electrode materials, metal (*e.g.*, copper or silver) powders have been intentionally dispersed on the electrode materials to improve the electronic conductivity.[30] So the presence of Co should be beneficial for the lithium-storage performance of the composite even if it is inactive toward lithium. The Co segments were also monitored in our TEM experiments to show how they response to the electrochemical process.

Figure 2 and movies S1 and S2 (in the Supporting Information) show the typical morphological evolution

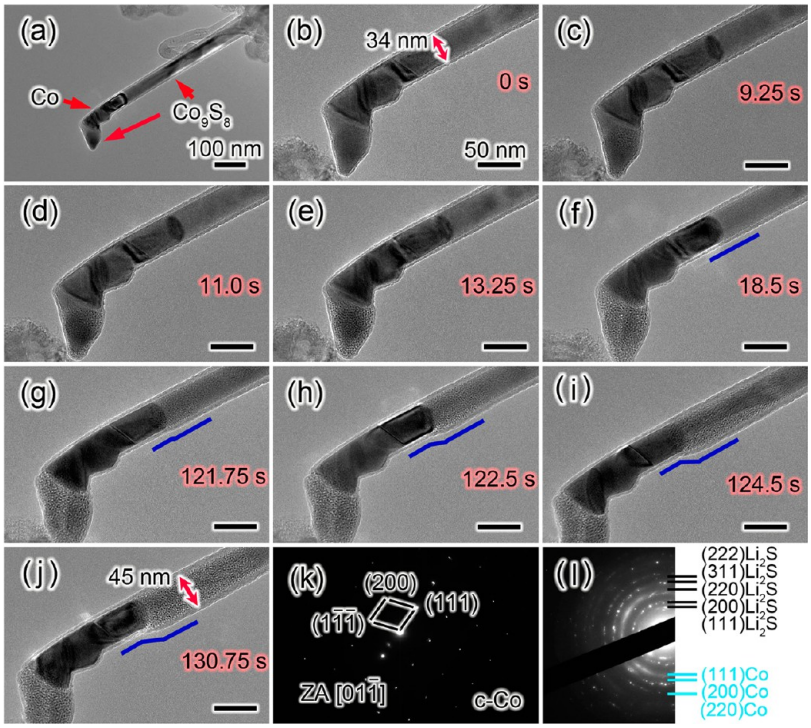

Figure 2. Time-resolved TEM images from video frames show direct electrochemical lithiation process of an individual Co_9S_8/Co-filled CNT with a carbon cap on the end. (a) The selected Co_9S_8/Co-filled CNT. (b) The contact of the CNT with Li/Li_2O electrodes to initiate the lithiation. (c−j) Time sequence of the lithiation process of the Co_9S_8/Co-filled CNT. (k) EDP of the pure Co filler after lithiation showing no phase transformation. (h) EDP of the lithiated Co_9S_8 nanowire showing the obvious phase conversion to Co and Li_2S. The blue lines in (f−j) denote the change of CNT diameter. All scale bars are 50 nm.

and phase transformation of an individual Co_9S_8/Co-filled CNT with closed end during the first lithiation process. Figure 2a depicts the pristine CNT before lithiation. The filler in this CNT consisted of three segments: a Co_9S_8 tip, a Co segment in the middle, and a long Co_9S_8 nanowire. The diameter of the Co_9S_8 nanowire within the CNT was 34 nm and the thickness of the CNT shell was about 5.4 nm. As the front surface of the Li_2O electrolyte touched the CNT (Figure 2b), the lithiation process was initiated by applying a negative potential of −0.1 V to the CNT with respect to the Li electrode. At 9.25 s (Figure 2c), a mild change could be observed in the Co_9S_8 tip in comparison to the image in Figure 2b, revealing the occurrence of lithiation. CNTs synthesized by the CVD method generally have many defects and the lithium ions can penetrate the CNT walls easily.[28,31,32] As the lithiation proceeded (see Figure 2d−f), the Co_9S_8 tip turned to gray grainy texture, and the filled CNT expanded in both axial and radial directions. The Co_9S_8 tip was completely lithiated with a noticeable volume expansion within 18.5 s (Figure 2f). Obvious electrochemical lithiation of the Co_9S_8 nanowire behind the Co segment was observed at 121.75 s, as confirmed in Figure 2g. We found no morphological evolution was detected for the Co segment. The corresponding EDP of the Co segment after lithiation was shown in Figure 2k, which was still identified as the cubic Co (JCPDF card No. 15−0806), suggesting no phase transformation occurred to the Co segment. The continuous lithiation of the Co_9S_8 nanowire was revealed by the change of the texture and the volume expansion of the Co_9S_8 filler in the TEM images (Figure 2g−i). After the full lithiation, the filler expanded to 45 nm in diameter (shown in Figure 2j). Interestingly, we observed anisotropic strain for the CNT with an axial elongation of 4.5% and a radial expansion of 32.4%. Correspondingly, the volume expansion of the Co_9S_8 filler is about 83.2% after the first lithiation process (details for the volume calculation are provided in the Supporting Information). The spacing of the (0002) plane of the CNT was increased from 3.4 to ∼3.6 Å, indicating the insertion of Li^+ into the graphite layers; the result is similar to the interlayer expansion observed in literature.[28] The EDP confirmed the phase transformation from single crystalline Co_9S_8 to mixed phases of Co and Li_2S (Figure 2l) after full lithiation. According to the TEM analysis, it can be concluded that numerous Co nanograins of 2−3 nm were formed and embedded in the resultant Li_2S matrix after the lithiation process. The electrochemical reaction of Co_9S_8 in LIBs can be expressed as $Co_9S_8 + 16Li^+ + 16e^- \rightarrow 9Co + 8Li_2S$. The lithiation reaction pertains to the conversion mechanism as reported for metal oxides.[33]

Two kinds of Co_9S_8/Co-filled CNTs were found in the products in terms of the closed or open tips. The lithiation behaviors of a filled CNT with closed ends were revealed in Figure 2. However, the Co_9S_8/Co-filled

CNT with an open end showed significantly different electrochemical behaviors as shown in Figure 3 and movie S3 in the Supporting Information. The pristine-filled CNT had an open tip with a diameter of 128 nm as shown in Figure 3a. The lithiation process was initiated by applying a potential of −0.1 V to the CNT electrode. After reaction for 18 s, an obvious lithiation was detected in the contact region of Co_9S_8 with the Li_2O electrolyte. The lithiation along the axial direction resulted in a gray-contrasted end (marked with the red arrow in Figure 3b). Figure 3c−g shows the elongation and extrusion of the lithiated filler, suggesting the axial elongation of filler is dominant for the open CNT. Note that the reaction front (Figure 3c), marked with red arrows and dashed lines, always kept a conical shape during the lithiation process, indicating that the Li^+ ions diffused mainly through CNT shell. The Co_9S_8 nanowire was divided into two segments with different contrasts by the reaction front during the lithiation, including the original Co_9S_8 filler on the right and the lithiated section on the left. The CNT showed weakly detectable radial expansion, and the lithiated nanowire was gradually extruded out of the open end of the CNT to relieve the volume expansion. Movie S4 in the Supporting Information shows the fast outward-moving of the lithiated filler. Similar to the lithiation process in the Co_9S_8/Co-filled CNT with closed ends, the lithiation in the open CNT can also cross the metal Co block to proceed in the second Co_9S_8 segment. It is noteworthy to mention that the Co block was pushed out toward the open end of the CNT owing to the expansion and extrusion of the second lithiated Co_9S_8 segment (denoted by blue arrow in Figure 3h). After the full lithiation process, the CNT showed a radial expansion of 4% due to the intercalation of Li^+ within the graphite layer and an undetectable axial elongation. The nanowire filler remained similar in diameter while showed a huge axial elongation of 94.2%. This was in contrast to the lithiation of filled CNT with carbon cap, in which the axial elongation was suppressed, while large radial expansion was observed. The volume expansion of the Co_9S_8 filling (94.2%) in open CNT is much larger than that (~83.2%) in a closed CNT with carbon cap, which is due to the mechanical constraint of the closed carbon shell. About 94.2% of the lithiated filler was extruded out of the open end of CNT. The comparison of these two types of CNTs reveals that a complete encapsulation of the metal sulfide (or oxide) by CNT is advantageous for the structural stability as anode materials in LIBs. It is worthy to mention that the CNT shells of Co_9S_8/Co-filled CNT show no evident fracture after lithiation in both cases and are distinguished from the amorphous carbon shells coated on SnO_2 nanowire. It was reported that the continuous carbon layer coated on SnO_2 nanowire was broken into tiny pieces in the axial direction after charging.[34] The difference can be ascribed to the superior strength of the graphitized CNT (~130 GPa) as compared to amorphous carbon (~3 GPa).[35]

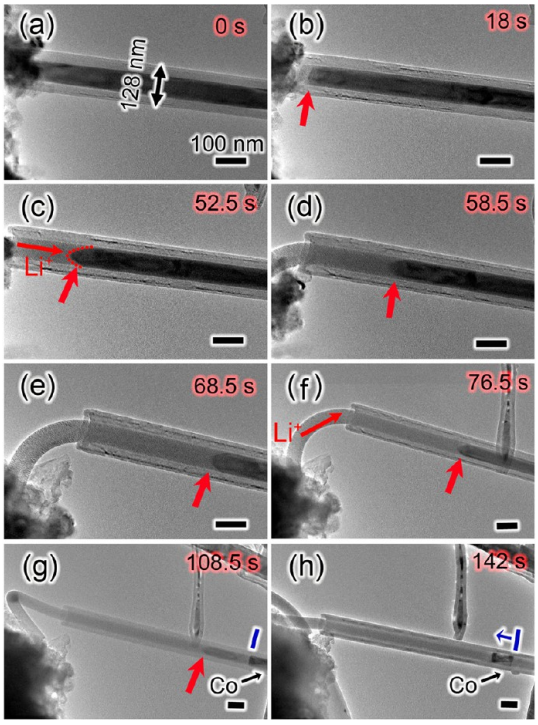

Figure 3. Time-resolved TEM images from video frames show the electrochemical lithiation process of an individual Co_9S_8/Co-filled CNT with an open end. The lithiation leads to the extrusion of the lithiated filler out of the CNT due to volume expansion. (a) The selected Co_9S_8/Co-filled CNT as working electrode. (b−h) Time sequence of lithiation process of Co_9S_8/Co-filled CNT, showing the nanowire filler was gradually extruded out of the open end of CNT during lithiation. The red dashed curve and arrows demonstrate the reaction front. The blue arrow in (h) denotes the moving direction of the Co segment. All scale bars are 100 nm.

To further reveal the microstructures of the lithiated Co_9S_8/Co-filled CNT without a carbon cap, TEM and electron energy-loss spectroscopy (EELS) analysis were performed. Figure 4a is a TEM image of a lithiated Co_9S_8/Co-filled CNT, showing the lithiated nanowire filler with a length of ~424 nm was extruded out of the open end of the CNT. High-magnification TEM images of this lithiated Co_9S_8/Co-filled CNT are displayed in Figure 4b,c. The diameter of the lithiated Co_9S_8 filler extruded out of the open end of the CNT is ~86.3 nm, which is slightly larger than that of the lithiated Co_9S_8 filler (~83.9 nm) within the carbon shells as shown in Figure 4b, further confirming the mechanical constraint of the carbon shells to the volume expansion of the Co_9S_8 filler. Interestingly, the extended nanowire is not bare but coated with a thin carbon shell besides an outermost Li_2O layer. The clear fringes with spacing of 0.36 nm, corresponding to the lithiated graphite layers, can be observed in Figure 4c. The EELS spectrum recorded from the extended nanowire is shown in Figure 4d, indicating the presence of

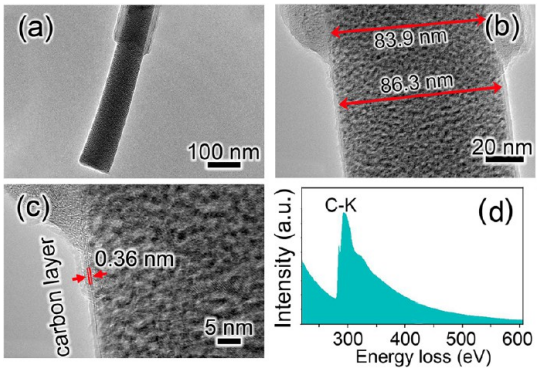

Figure 4. (a) TEM image and (b, c) magnified TEM images of a lithiated Co_9S_8-filled CNT with an open end. (d) EELS spectrum of the extended nanowire showing the presence of carbon.

C (C−K edge: 283.8 eV). TEM and EELS analysis demonstrate the shell coated on the extended nanowire is graphite layer, which should be pulled out from the CNT shells by the outward-moving lithiated filler. Multiwall CNTs comprise of concentric cylindrical shells of graphite-like sp^2-bonded carbon, where the intershell interaction is predominantly van der Waals and could be weakened with the lithium insertion. Thus, the dragging out of the carbon shell from CNT in our experiment could be attributed to the lithiation-induced decrease of carbon−carbon bonds[28] and the large hoop stress formed in the multiwall CNT owing to the swelling of filler.[35,36] The presence of carbon shell on the extended nanowire filler is unexpected but definitely advantageous to the electrochemical performance since it can improve the electrical conductivity of electrode materials.

The cyclability performance is crucial for LIB electrode materials. In our experiments, the lithiation−delithiation cycling behaviors of a Co_9S_8/Co-filled CNT were examined using *in situ* TEM. A filled CNT with a carbon cap on the end was first selected as the nanoscale electrode (Figure 5a). There were two segments in the CNT tip which were labeled with A and B. Inset of Figure 5a shows the corresponding EDP of part B, confirming it is single-crystalline Co particle along the [0 1 −1] zone axis. The HRTEM image of part A is given in Figure 5b; the clear lattice fringes of carbon shells suggest the high level of graphitization of the CNT. The fast Fourier transform (FFT) image of the HRTEM is given in the inset of Figure 5b, confirming the part A is Co_9S_8. After first lithiation with a bias of −0.1 V (Figure 5c), the diameter of CNT tip with part A (filled Co_9S_8 section) increased to 118 nm from 96 nm while the Co filler remained intact and maintained 40 nm in diameter. The lithiation reaction of Co_9S_8 was clearly observed while the Co part showed strong resistance to the lithiation. The potential was reversed to +3 V to initiate the delithiation after the lithiation was completed. The part A shrank gradually and decreased to about 111 nm in diameter (Figure 5d),

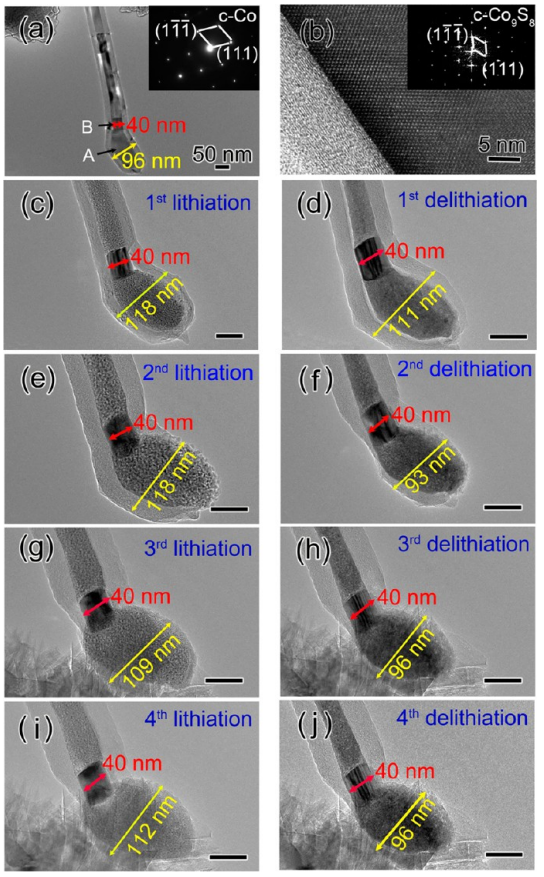

Figure 5. Lithiation−delithiation cycles of a single Co_9S_8/Co-filled CNT electrode. (a) Pristine CNT with a Co filler of 40 nm in diameter and a Co_9S_8-filled tip of 96 nm in diameter. The inset is the EDP of part B confirming pure Co phase. (b) HRTEM image of part A, and the inset is the FFT image indicating the Co_9S_8. (c, d) First lithiation−delithiation cycle. (e−j) The second, third, and fourth lithiation−delithiation cycles showing the same behaviors as the first cycle, demonstrating the good cyclability of the Co_9S_8/Co-filled CNT with closed end. All scale bars are 50 nm.

which suggested that the Li^+ ions had been extracted from the lithiated Co_9S_8. Note that there were some blank space observed between the filling core and the CNT shell, suggesting the contraction of Co_9S_8 was much severer than that of CNT shell. After the first cycle, repeated lithiation−delithiation cycles of the selected CNT were conducted by alternately reversing the applied potential between −0.1 V and +3.0 V, as shown in Figure 5e−j. Interestingly, the repeated expansion and contraction of Co_9S_8 nanowire was observed, and the Co filler was unchanged and maintained its diameter of about 40 nm during the four lithiation−delithiation cycles. We found that the CNT tip could damage and fracture after several cycles. Similar breakdown was also observed during the lithiation of graphene sheet.[25] Because the damages were only observed in the contacting end of CNT with the solid electrolyte, two possible reasons are proposed here. First, the lithiated CNTs are brittle due to the combined effects of mechanical and chemical weakening of the C−C bonds

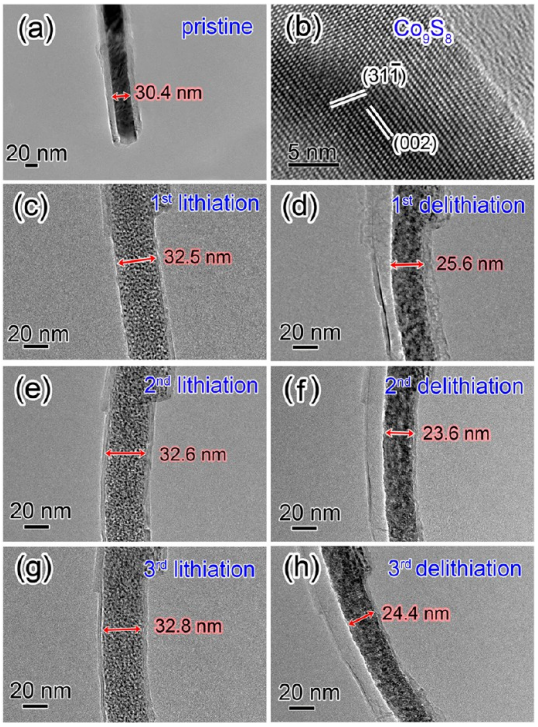

Figure 6. Lithiation−delithiation cycles of a Co_9S_8-filled CNT with an open end. (a) Pristine CNT with Co_9S_8 filling of 30.4 nm in diameter. (b) HRTEM image of the Co_9S_8 filler. (c, d) First lithiation−delithiation cycle. (e−h) The second and third lithiation−delithiation cycles showing the repeated expansion and contraction of the nanowire filler.

induced by lithium insertion.[28] Second, there are strong compression and friction forces applied to the contacting region during the lithiation, which cause the fracture of the embrittled CNT tip. We expect that this kind of damage can be avoided in real battery with liquid electrolyte.

Furthermore, the lithiation−delithiation cycling behaviors of an individual filled CNT with an open end were investigated using the *in situ* TEM. Figure 6a shows the TEM image of the pristine Co_9S_8-filled CNT. The Co_9S_8 filler is 30.4 nm in diameter, and its crystalline structure can be confirmed by HRTEM image in Figure 6b. After the first lithiation process with a bias of −0.1 V, the lithiated filler was extruded out from the CNT open tip, and the diameter of the filler slightly increased to 32.5 nm (Figure 6c). Then the potential was reversed to +3 V to initiate the delithiation. This filler shrank and decreased to about 25.6 nm in diameter (Figure 6d), which suggested that the Li^+ ions were extracted from the lithiated filler. The lithiated filler were found to exhibit obvious radial contraction while its length showed negligible change. The extended filler could not retract into the CNT and, thus, left a large empty space within the CNT. It should be pointed out that a few layers of graphite shells were also dragged out from the CNT by the lithiated filler during the lithiation process. The graphite shells can be clearly observed after the delithiation, which resulted

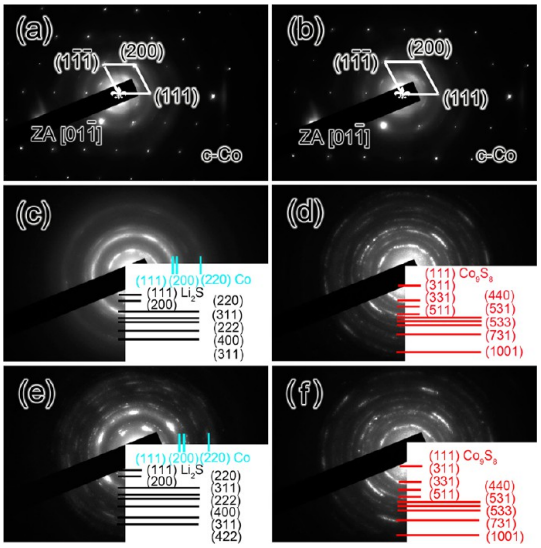

Figure 7. Identification of various phases transformation of Co_9S_8/Co-filled CNT during lithiation−delithiation cycles. EDPs of lithiated (a) and delithiated Co filler (b) showing that the Co segment maintained the pristine phase during cycles. EDPs of the Co_9S_8 filler in CNT electrode after the first lithiation (c), first delithiation (d), the second lithiation (e), and second delithiation (f).

in empty room inside graphite shells owing to shrinkage of the filler. The repeated expansion and contraction of the nanowire filler was observed in the second and third cycles as shown in Figure 6e−h, indicating a good cyclability after the first cycle. The encapsulation of original CNT and the drawn-out graphite shells to the Co_9S_8 filler are critical for achieving good cyclability.

The morphological changes of the filled CNT electrode during lithiation−delithiation cycles have been demonstrated in Figures 5 and 6. To reveal the phase transformation during the cycles, the corresponding EDPs were recorded on the Co_9S_8/Co-filled CNT electrode as shown in Figure 7. First, the cycling behaviors of the segment B as shown in Figure 5a were investigated. The pristine segment B was single-crystalline cubic Co along the [0, 1, −1] zone axis, as revealed by the EDP in the inset in Figure 5a. After the full lithiation process, no phase transformation was detected, and the corresponding EDP was given in Figure 7a and can still be indexed as single-crystalline cubic Co. The delithiation process was initiated by applying a bias of +3 V. The Co filler maintained its original structure, as confirmed by the corresponding EDP in Figure 7b. The structure evolution of Co_9S_8 filler were further examined, and the corresponding EDPs of the filler during the first two lithiation−delithiation cycles are displayed in Figure 7c−f. Figure 7c displays the EDP of the Co_9S_8 filler after the first lithiation, and the diffraction rings can be well indexed to cubic Co and Li_2S, corresponding to the electrochemical reaction $Co_9S_8 + 16Li^+ + 16e^- \rightarrow 9Co + 8Li_2S$. Figure 7d displays the EDP of the first delithiated filler, which can be well indexed to Co_9S_8 phase, suggesting the reversible

conversion between Co_9S_8 and Co nanograins during the charge–discharge cycles. The extraction of Li^+ ions from the mixture of Co nanograins and Li_2S resulted in the formation of Co_9S_8 phase. Here we want to emphasize that there were two kinds of Co in the lithiated CNT: one is the original Co filler (in segment B) and the other is the resultant Co nanograins in the lithiated product. The latter is electrochemically active and can be converted to Co_9S_8, while the former is fully inert. The difference might be attributed to the crystal size and quantum size effects of Co nanograins (2–3 nm). In the second lithiation–delithiation cycle, the same structure conversion was also observed. The results reveal that the phase transformation between Co_9S_8 and Co is fully reversible during lithiation–delithiation cycles.

According to the *in situ* TEM study by constructing a nano-LIB device inside the TEM, the electrochemical lithiation processes of Co_9S_8/Co-filled CNTs proceed as illustrated in Figure 8. Two kinds of electrochemical behaviors are proposed in terms of the different CNT structures. As for the filled CNT with carbon cap, the corresponding lithiation process is shown in Figure 8a. The pristine Co_9S_8/Co-filled CNT is initially straight and uniform in diameter. As the reaction front (marked by the red dashed lines) propagates from the left to the right, the CNT swells gradually. Due to the presence of short Co segment, the CNT shows intermittent expansion. Because of the suppression of the carbon cap, a small axial elongation and a significant radial expansion are presented. After full lithiation, a single-crystalline Co_9S_8 nanowire transforms to a multicrystalline nanowire consisting of numerous Co nanograins embedded within Li_2S matrix. Figure 8b illustrates the microstructural evolution during the first lithiation of a Co_9S_8/Co-filled CNT with an open end. Different from the closed CNT, as the reaction front propagates, the lithiated filler elongates and is extruded out of the CNT while still kept the similar diameter. Therefore, weakly radial expansion is demonstrated while axial elongation is notable for the lithiation of filled CNT with an open end. Co segment can move with the extending of the lithiated filler. In particular, the extended filler was still encapsulated with a graphite shell pulled out from the original CNT due to the weak intertube van der Waals force within the CNT. The volume expansion of the filler is 94.2% for the open CNT, while it reduces to 83.2% for the closed CNT due to the mechanical confinement of the graphite shells. Besides, the radial expansion of the open CNT is about 4%, which can be attributed to the intrinsic expansion due to the Li^+ intercalation; the radial expansion of the closed CNT is found to be 32.4%, so about 28.4% of the radial expansion of the CNT should be caused by the internal pressure owing to the volume expansion of the filler. During the charge–discharge cycles, the Co segment remains intact while the Co_9S_8 filler shows a reversible

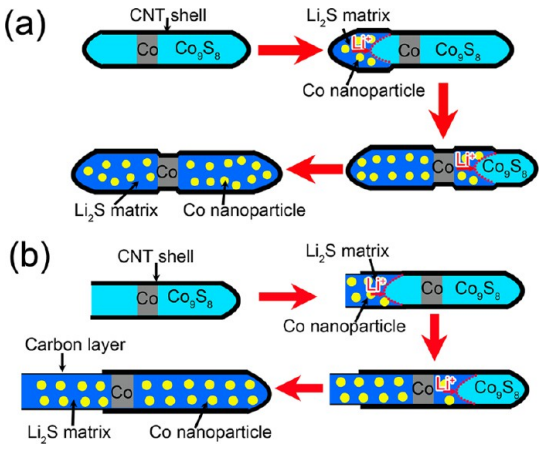

Figure 8. Schematic drawing shows the electrochemical lithiation of a Co_9S_8/Co-filled CNT with closed ends (a) and an open end (b).

electrochemical conversion between Co_9S_8 and Co/Li_2S. The volume expansion (94.2%) of the lithiated Co_9S_8 filler in an open CNT is much larger than that (~83.2%) in a closed CNT, which seems unintelligible because they are the same material (i.e., the mixture of Co and Li_2S nanocrystals). To explain this phenomenon, a typical TEM image of a lithiated CNT is shown in Figure S2 in the Supporting Information. It can be seen clearly that the average diameter of the lithiated filler within the CNT is ~95.3 nm, while the diameter of the filler extruded out of the open CNT is 98.1 nm. The different diameters of the lithiated fillers inside and outside the CNT suggest that the mechanical constraint of the carbon shells to the diameter change of the lithiated filler is profound. The extended filler out of the CNT could have a lower density as compared to the filler within the CNT sheath even if they are the same material. The lower density of the extended filler is probably caused by the different Li^+ transport mechanism. The Li^+ ions diffuse mainly along the CNT in the beginning of lithiation, however, when the lithiation proceeds, the CNT shell disconnects from the solid electrolyte and the Li^+ ions have to diffuse through the extended filler as indicated in Figure S2. The rapid diffusion of numerous Li^+ ions may cause the formation of transport tunnels inside the lithiated filler, which can consequently reduce the density of the lithiated filler and increase the volume. In the meantime, the repulsion of positively charged Li^+ ions may also contribute to the volume expansion of the filler outside the CNT. Therefore, different diameters are observed for the lithiated filler around the tip of CNT in the TEM images.

CONCLUSION

In summary, the electrochemical lithiation–delithiation behaviors of individual Co_9S_8/Co-filled CNTs were investigated using *in situ* TEM by constructing a nano-LIB device inside a TEM. We have revealed the effect of

the carbon cap on the lithium-storage behaviors of filled CNT. The Co_9S_8/Co-filled CNT with an open end shows a notable axial elongation of the lithiated filler by 94.2%, while the filled CNT with closed ends shows a major radial expansion of 32.4%. Intermittent swelling has been observed in the closed CNT due to the presence of Co segment, which is stable in the electrochemical cycles. During the lithiation process, single-crystalline Co_9S_8 nanowire converts to multicrystalline nanowire consisting of Co nanograins and Li_2S matrix, and the reversible phase conversion between Co_9S_8 and nanosized Co is revealed during the multiple cycles. These results reveal that the filled CNT with closed ends is favorable for the electrode material to maintain their original shape during lithiation–delithiation cycles, which can reduce irreversible changes, maintain good contact between the filling and the CNT shell, and thus benefit the electrochemical lithium-storage performance. The filler inside a CNT with open end will be extruded out of the CNT due to the large volume expansion after lithiation. Fortunately, the extruded filler will be confined by a graphite shell pulled out from the CNT by the extruded filler, and the graphite shell ensures the stability of the extruded filler during the next lithiation–delithiation cycles. This finding will be valuable for designing high-performance, CNT-based anode materials for LIBs.

EXPERIMENTAL SECTION

The *in situ* nanoscale electrochemical experiments were conducted inside a JEM–2100F transmission electron microscope (TEM) using a Nanofactory TEM-scanning tunneling microscopy (STM) holder. To construct the nano-LIB, Co_9S_8/Co-filled CNT sample was attached to a blunt Au wire (0.25 mm diameter), serving as the working electrode. A sharp tungsten (W) STM tip was used to scratch the Li metal surface to fetch some fresh Li inside a glovebox filled with argon. The layer of Li on the tip of the W rod served as the counter electrode and lithium source. Both the CNT and lithium electrodes were mounted onto a Nanofactory STM-TEM holder, which was quickly transferred into the TEM column. A native Li_2O layer formed on the surface of the Li metal due to the exposure to air, which was served as the solid-state electrolyte to allow the transport of Li^+ ions. The Li_2O/Li electrode attached to the mobile STM probe was driven to contact the CNT electrode inside the TEM. Lithiation took place after a negative bias was applied to the Co_9S_8/Co-filled CNT electrode with respect to the lithium electrode to drive Li^+ to transport through the solid-state Li_2O layer, and the bias was then reversed to positive to facilitate delithiation. During the experiments the electron beam was blanked except for short time beam exposure for imaging to minimize the electron beam irradiation effect during the reaction.

Conflict of Interest: The authors declare no competing financial interest.

Acknowledgment. This work was supported by the Program for New Century Excellent Talents in University of Ministry of Education of China (NCET-11-1081), the National Science Foundation of China (No. 21203168), and the American Chemical Society Petroleum Research Fund under grant 51766-ND10.

Supporting Information Available: Four videos showing the lithiation process of individual Co_9S_8/Co-filled CNTs. Details for the calculation of volume expansion of Co_9S_8 filler and TEM image showing the diameter change of a lithiated filler. This material is available free of charge *via* the Internet at http://pubs.acs.org.

REFERENCES AND NOTES

1. Armand, M.; Tarascon, J. M. Building Better Batteries. *Nature* **2008**, *451*, 652.
2. Wang, B.; Chen, J. S.; Wu, H. B.; Wang, Z.; Lou, X. W. Quasiemulsion-Templated Formation of α-Fe_2O_3 Hollow Spheres with Enhanced Lithium Storage Properties. *J. Am. Chem. Soc.* **2011**, *133*, 17146–17148.
3. Tarascon, J. M.; Armand, M. Issues and Challenges Facing Rechargeable Lithium Batteries. *Nature* **2001**, *414*, 359–367.
4. Lou, X. W.; Archer, L. A.; Yang, Z. C. Hollow Micro-/Nanostructures: Synthesis and Applications. *Adv. Mater.* **2008**, *20*, 3987–4019.
5. Service, R. F. Getting There. *Science* **2011**, *332*, 1494–1496.
6. Wang, Z. Y.; Zhou, L.; Lou, X. W. Metal Oxide Hollow Nanostructures for Lithium-Ion Batteries. *Adv. Mater.* **2012**, *24*, 1903–1911.
7. Whittingham, M. S. Electrical Energy Storage and Intercalation Chemistry. *Science* **1976**, *192*, 1126–1127.
8. Zhang, D.; Mai, Y. J.; Xiang, J. Y.; Xia, X. H.; Qiao, Y. Q.; Tu, J. P. FeS_2/C Composite as an Anode for Lithium Ion Batteries with Enhanced Reversible Capacity. *J. Power Sources* **2012**, *217*, 229–235.
9. Ni, S. B.; Yang, X. L.; Li, T. Fabrication of a Porous NiS/Ni Nanostructured Electrode *via* a Dry Thermal Sulfuration Method and Its Application in a Lithium Ion Battery. *J. Mater. Chem.* **2012**, *22*, 2395–2397.
10. Lu, Y.; Tu, J. P.; Xiong, Q. Q.; Xiang, J. Y.; Mai, Y. J.; Zhang, J.; Qiao, Y. Q.; Wang, X. L.; Gu, C. D.; Mao, S. X. Controllable Synthesis of a Monophase Nickel Phosphide/Carbon (Ni_5P_4/C) Composite Electrode *via* Wet-Chemistry and a Solid-State Reaction for the Anode in Lithium Secondary Batteries. *Adv. Funct. Mater.* **2012**, *22*, 3927–3935.
11. Wang, J.; Ng, S. H.; Wang, G. X.; Chen, J.; Zhao, L.; Chen, Y.; Liu, H. K. Synthesis and Characterization of Nanosize Cobalt Sulfide for Rechargeable Lithium Batteries. *J. Power Sources* **2006**, *159*, 287–290.
12. Huang, J. Y.; Zhong, L.; Wang, C. M.; Sullivan, J. P.; Xu, W.; Zhang, L. Q.; Mao, S. X.; Hudak, N. S.; Liu, X. H; Subramanian, A.; *et al. In Situ* Observation of the Electrochemical Lithiation of a Single SnO_2 Nanowire Electrode. *Science* **2010**, *330*, 1515–1520.
13. Liu, X. H.; Liu, Y.; Kushima, A.; Zhang, S. L.; Zhu, T.; Li, J.; Huang, J. Y. *In Situ* TEM Experiments of Electrochemical Lithiation and Delithiation of Individual Nanostructures. *Adv. Energy Mater.* **2012**, *2*, 722–741.
14. Kushima, A.; Liu, X. H.; Zhu, G.; Wang, Z. L.; Huang, J. Y.; Li, J. Leapfrog Cracking and Nanoamorphization of ZnO Nanowires during *In Situ* Electrochemical Lithiation. *Nano Lett.* **2011**, *11*, 4535–4541.
15. Xie, D.; Yuan, W. W.; Dong, Z. M.; Su, Q. M.; Zhang, J.; Du, G. H. Facile Synthesis of Porous NiO Hollow Microspheres and Its Electrochemical Lithium-Storage Performance. *Electrochim. Acta* **2013**, *92*, 87–92.
16. Wu, Z. S.; Ren, W. C.; Xu, L.; Li, F.; Cheng, H. M. Doped Graphene Sheets as Anode Materials with Super High Rate and Large Capacity for Lithium Ion Batteries. *ACS Nano* **2011**, *5*, 5463–5471.
17. Peng, C. X.; Chen, B. D.; Qin, Y. Facile Ultrasonic Synthesis of CoO Quantum Dot/Graphene Nanosheet Composites with High Lithium Storage Capacity. *ACS Nano* **2012**, *6*, 1074–1081.
18. Ban, C. M.; Wu, Z. C.; Gillaspie, D. T.; Chen, L.; Yan, Y. F.; Blackburn, J. L.; Dillon, A. C. Nanostructured Fe_3O_4/SWNT Electrode: Binder-Free and High-Rate Li-Ion Anode. *Adv. Mater.* **2010**, *22*, E145–E149.
19. Ko, S.; Lee, J. I.; Yang, H. S.; Park, S.; Jeong, U. Mesoporous CuO Particles Threaded with CNTs for High-Performance Lithium-Ion Battery Anodes. *Adv. Mater.* **2012**, *24*, 4451–4456.

20. Shi, W. H.; Zhu, J. X.; Rui, X. H.; Cao, X. H.; Chen, C.; Zhang, H.; Hng, H. H.; Yan, Q. Y. Controlled Synthesis of Carbon-Coated Cobalt Sulfide Nanostructures in Oil Phase with Enhanced Li Storage Performances. *ACS Appl. Mater. Interfaces* **2012**, *4*, 2999–3006.
21. Key, B.; Morcrette, M.; Tarascon, J. M.; Grey, C. P. Pair Distribution Function Analysis and Solid State NMR Studies of Silicon Electrodes for Lithium Ion Battery: Understanding the (De)Lithiation Mechanisms. *J. Am. Chem. Soc.* **2011**, *133*, 503–512.
22. Li, J.; Dahn, J. R. An *In Situ* X-ray Diffraction Study of the Reaction of Li with Crystalline Si. *J. Electrochem. Soc.* **2007**, *154*, A156–A161.
23. Chen, D.; Indris, S.; Schulz, M.; Gamer, B.; Mönig, R. *In Situ* Scanning Electron Microscopy on Lithium-Ion Battery Electrodes Using an Ionic Liquid. *J. Power Sources* **2011**, *196*, 6382–6387.
24. Wang, C. M.; Xu, W.; Liu, J.; Zhang, J. G.; Saraf, L. V.; Arey, B. W.; Choi, D.; Yang, Z. G.; Xiao, J.; Thevuthasan, S.; et al. *In Situ* Transmission Electron Microscopy Observation of Microstructure and Phase Evolution in a SnO_2 Nanowire during Lithium Intercalation. *Nano Lett.* **2011**, *11*, 1874–1880.
25. Su, Q. M.; Chang, L.; Zhang, J.; Du, G. H.; Xu, B. S. *In Situ* TEM Observation of the Electrochemical Process of Individual CeO_2/Graphene Anode for Lithium Ion Battery. *J. Phys. Chem. C* **2013**, *117*, 4292–4298.
26. Ghassemi, H.; Au, M.; Chen, N.; Heiden, P. A.; Yassar, R. S. *In Situ* Electrochemical Lithiation/Delithiation Observation of Individual Amorphous Si Nanorods. *ACS Nano* **2011**, *5*, 7805–7811.
27. Su, Q. M.; Xie, D.; Zhang, J.; Du, G. H.; Xu, B. S. *In Situ* Transmission Electron Microscopy Observation of the Conversion Mechanism of Fe_2O_3/Graphene Anode during Lithiation−Delithiation Process. *ACS Nano* **2013**, *7*, 9115–9121.
28. Liu, Y.; Zheng, H.; Liu, X. H.; Huang, S.; Zhu, T.; Wang, J. W.; Kushima, A.; Hudak, N. S.; Huang, X.; Zhang, S. L. Lithiation-Induced Embrittlement of Multiwalled Carbon Nanotubes. *ACS Nano* **2011**, *5*, 7245–7253.
29. Du, G. H.; Li, W. Z.; Liu, Y. Q. Filling Carbon Nanotubes with Co_9S_8 Nanowires through *In Situ* Catalyst Transition and Extrusion. *J. Phys. Chem. C* **2008**, *112*, 1890–1895.
30. Croce, F.; D'Epifanio, A.; Hassoun, J.; Deptula, A.; Olczac, T.; Scrosati, B. A Novel Concept for the Synthesis of an Improved $LiFePO_4$ Lithium Battery Cathode. *Electrochem. Solid-State Lett.* **2002**, *5*, A47–A50.
31. Meunier, V.; Kephart, J.; Roland, C.; Bernholc, J. *Ab Initio* Investigations of Lithium Diffusion in Carbon Nanotube System. *Phys. Rev. Lett.* **2002**, *88*, 075506.
32. Yang, Z. H.; Wu, H. Q. Electrochemical Intercalation of Lithium into Carbon Nanotubes. *Solid State Ionics* **2001**, *143*, 173–180.
33. Poizot, P.; Laruelle, S.; Grugeon, S.; Dupont, L.; Tarascon, J. M. Nano-Sized Transition Metal Oxides as Negative Electrode Materials for Lithium-Ion Batteries. *Nature* **2000**, *407*, 496–499.
34. Zhang, L. Q.; Liu, X. H.; Liu, Y.; Huang, S.; Zhu, T.; Gui, L. J.; Mao, S. X.; Ye, Z. Z.; Wang, C. M.; Sullivan, J. P.; *et al.* Controlling the Lithiation-Induced Strain and Charging Rate in Nanowire Electrodes by Coating. *ACS Nano* **2011**, *5*, 4800–4809.
35. Gu, M.; Li, Y.; Li, X. L.; Hu, S. Y.; Zhang, X. W.; Xu, W.; Thevuthasan, S.; Baer, D. R.; Zhang, J. G.; Liu, J.; et al. *In Situ* TEM Study of Lithiation Behavior of Silicon Nanoparticles Attached to and Embedded in a Carbon Matrix. *ACS Nano* **2012**, *6*, 8439–8447.
36. Wang, J. W.; Liu, X. H.; Zhao, K. J.; Palmer, A.; Patten, E.; Burton, D.; Mao, S. X.; Suo, Z. G.; Huang, J. Y. Sandwich-Lithiation and Longitudinal Crack in Amorphous Silicon Coated on Carbon Nanofibers. *ACS Nano* **2012**, *6*, 9158–9167.